PAPER

Check for updates

Computer-aided development of bio-inspired routes to highly ordered green mesoporous silica†

Tom Stavert,[a] Carlos Brambila,[b] Siddharth V. Patwardhan [ID] *[b] and Miguel Jorge [ID] *[a]

Bio-inspired routes to producing porous silica materials offer great potential to make the currently adopted synthesis routes more sustainable through the use of milder synthesis conditions, short reaction times and non-toxic reagents. Ordered mesoporous silica (OMS) synthesis would benefit greatly from these green synthesis routes, but a lack of mechanistic understanding of bio-inspired silica synthesis makes applying these approaches directly to OMS synthesis challenging. In this work, we apply a unique combination of design of experiments and multi-scale modelling to better understand how the structure of OMS can be controlled by manipulating synthesis conditions, with a focus on using bio-inspired additives to facilitate mild synthesis conditions and improve yield, whilst maintaining highly ordered pore structures. Our simulation results show that the silica/surfactant ratio plays a crucial role in the promotion of ordered mesophases by controlling the delicate balance between charge-matching interactions at the surface of silica/surfactant micelles. However, a trade-off is observed between the degree of order and the product yield, which decreases as the silica concentration increases. This problem can be addressed by the inclusion of the bio-inspired additive pentaethylenehexamine, which we hypothesize to have a catalytic effect on the silica condensation reaction occurring at the silica/surfactant interface. Our results indicate that the properties of the material are determined by an interplay between self-assembly and reaction kinetics, such that ordered materials can be obtained by first allowing the mesophase to self-assemble at high pH, then rapidly lowering the pH in the presence of the bio-inspired additive to "lock-in" the mesostructure through silica polymerization. Based on these insights, we propose a novel synthesis route to produce highly ordered OMS materials more rapidly, under milder synthesis conditions and with higher yield than has been previously reported.

1 Introduction

Bio-inspired silica (BIS) is characterised by very mild synthesis conditions, which make it appealing from both an economical and environmental standpoint.[1,2] BIS makes use of simple organic amine-based "additives" to precipitate porous silica. Additives vary in complexity of structure and include amine-containing polymers (*e.g.* poly(L-lysine) (PLL), poly(allylamine) (PAA)), diamines, polyamines and amino acids (*e.g.* L-arginine, L-histidine, L-lysine).[3] The use of these additives allows the porosity of BIS to be controlled in a predictable manner, particularly in the case of polyamine molecules.[4] However, synthesis of BIS with ordered pores is still not possible, with materials possessing amorphous pores, predominantly in the microporous range (less than 2 nm in diameter).

In contrast, ordered mesoporous silica (OMS) materials (*e.g.* MCM-41,[5] SBA-15 [6]) have incredibly narrow pore size distributions. These properties make OMS incredibly effective in a broad variety of applications, including drug delivery,[7,8] biosensing,[9] bioimaging[10] and catalysis.[11] This is due to their well-ordered porous network, formed from a surfactant liquid crystal template that self-assembles in solution during synthesis. However, achieving this highly ordered porous structure currently involves the use of much harsher synthesis conditions than those employed for BIS synthesis. In particular, a typical synthesis of MCM-41 involves a lengthy hydrothermal treatment step to increase the mesoscopic regularity of pores, which takes place at high temperatures (up to 150 °C) making the process both time- and energy-intensive.[12] To our knowledge, only a handful of previous studies reported the synthesis of ordered MCM-41 materials at room temperature, but the evidence is somewhat contradictory. Lin *et al.*[13] used a "delayed neutralization" method, whereby acid was added after the silica

[a]Department of Chemical & Process Engineering, University of Strathclyde, 75 Montrose Street, Glasgow, G1 1XL, UK. E-mail: miguel.jorge@strath.ac.uk

[b]Department of Chemical and Biological Engineering, University of Sheffield, Mappin Street, Sheffield, S1 4LZ, UK. E-mail: s.patwardhan@sheffield.ac.uk

† Electronic supplementary information (ESI) available: Experimental results for all samples in tabular format; adsorption isotherms for all samples; X-ray diffraction patterns for all samples; description of uncertainty analysis; labelled graphs of analysed XRD patterns from literature; development and description of coarse-grained model for bio-inspired additives arginine and PEHA; description of ionisation model for silicates; full simulation details in tabular format; additional experimental results with discussion. See DOI: https://doi.org/10.1039/d5ta02010g

37044 | *J. Mater. Chem. A*, 2025, **13**, 37044–37062

This journal is © The Royal Society of Chemistry 2025

precursors (sodium silicate) and surfactants were allowed to self-assemble at high pH. They obtained MCM-41 materials at room temperature, but achieving a high degree of order required prolonged ageing of the synthesis solution over a period of several days. Cai *et al.*[14] reported the formation of highly ordered MCM-41 at room temperature from tetra-ethyl orthosilicate (TEOS), but only in a very narrow window of pH values and at a single relative ratio of silica to surfactant, which was 8 : 1. Results from a later study, however, suggest that hydrothermal treatment is necessary to produce MCM-41 materials with a high degree of order, such that they show well resolved XRD peaks at reflection lines (110) and (200).[15] Moreover, even in the study of Cai *et al.*, synthesis times of at least 2 hours were required.[14] The exact mechanisms by which well-ordered structures can be obtained and controlled without hydrothermal treatment remain unclear, and, at best, reaction times on the scale of hours are required.

BIS synthesis is much faster than OMS synthesis and takes place under milder conditions. For this reason, we hypothesised that bio-inspired additives can be used to promote the formation of OMS under milder conditions than those typically utilised for OMS synthesis.[12] Arginine was initially chosen due to its known importance in biological silica formation and its reported ability to accelerate bio-inspired silica synthesis.[3,16,17] However, conventional methods for producing amino acids (such as arginine) have known environmental drawbacks, so we also test other amine-containing bio-inspired additives, such as pentaethylenehexamine (PEHA), widely used in bio-inspired silica synthesis.[16] As the behaviour of bio-inspired additives in this system and their interactions with both templating surfactants and silica precursors are not well understood from a mechanistic perspective, we attempt to elucidate it through a combination of experiments and multi-scale modelling. Specifically, we aim to understand if and how bio-inspired additives may aid the formation of well-ordered mesoporous silica materials under ambient conditions, with the goal of enabling a more sustainable and scalable synthesis approach for OMS that does not rely on an energy-intensive hydrothermal treatment step or a lengthy ageing period. A design of experiments (DoE) approach is taken to identify which conditions impact the synthesis and resultant material properties, focusing on material porosity and morphology at the mesoscale (2–50 nm) as proxies for its performance in potential applications. Attention is also given to factors that influence the scalability and economics of the synthesis, for example the material yield and the quantity of reagents required for synthesis.[1] The experimental work is supported by coarse-grained molecular dynamics simulations of the co-operative self-assembly of the surfactant and silica precursor species, which gives rise to the resulting structure of these materials. Computational modelling provides an invaluable tool to gain a detailed understanding of the underlying mechanisms of self-assembly, which is hard to achieve experimentally.[18] These methods have previously been applied to study the early stages of OMS formation, showing the importance of silica species in promoting the aggregation of the surfactant phase, and specifically highlighting the role of multiply charged oligomers in the formation

of the hexagonal liquid crystal (HLC) template.[19–21] We have also previously combined modelling and experimental work to elucidate the synthesis mechanism of amine-templated materials.[22,23] Building on these successes, here we provide new insight into how bio-inspired additives interact with silica and surfactants, and how these interactions can influence the onset of order in mesoporous silica materials.

2 Methodology

2.1 Synthesis of mesoporous silica

Learning from the synthesis of BIS, we adopted a synthesis method that is similar in spirit to the "delayed neutralization" approach of Lin *et al.*[13] In a typical synthesis procedure, sodium metasilicate pentahydrate, $Na_2SiO_3 \cdot 5H_2O$ (Sigma-Aldrich ≥95.0%), cetyltrimethylammonium bromide (CTAB, Sigma-Aldrich ≥98%) and L-arginine (Sigma-Aldrich 99%) were dissolved in deionised water under constant stirring at room temperature. The initial pH was measured to ensure the resulting solution had a stable pH >13, which was the case for all experiments carried out here. A solution of 1.0 M hydrochloric acid was then added rapidly to the mixture under constant stirring to achieve the final desired pH (typically between 7 and 10) – we henceforth refer to this as simply the "pH", since it is one of our control variables. The pH was monitored using a pH probe throughout the reaction and maintained to within ± 0.05 of the synthesis pH after the initial addition of acid by dropwise addition of additional hydrochloric acid. Rapid precipitation was observed within seconds of acid addition, indicated by a visible increase in turbidity. The mixture was left under stirring for 5 minutes, at which point it was transferred to 50 mL conical centrifuge tubes. These were centrifuged for 7 minutes at 5000 rpm and the supernatant was discarded. The solid white precipitate was re-suspended in deionized water and shaken vigorously in order to wash the precipitate. The suspension was then centrifuged again. This washing procedure was repeated 3 times for each sample, and the conductivity of the supernatant for each wash was measured each time using a handheld conductivity probe to ensure a significant reduction of salts present in the supernatant by the final wash, below the detectability limit of the probe. The precipitate was then dried in an oven at 60 °C for 48 hours. The dried sample was weighed, and then placed in a furnace in a heat-proof crucible for 6 hours at 550 °C, obtaining the final mesoporous silica product which was then weighed. A diagram illustrating the synthesis procedure is shown in Fig. 1.

2.2 Design of experiments

The design of experiments (DoE) involves systematically changing input parameters (factors) to study how this affects output variables (responses), allowing for an understanding of the relationship between these factors and responses to be obtained. This procedure was applied to the synthesis of mesoporous silica following the method outlined in Section 2.1 to create a link between synthesis conditions and material properties. Initially, a two-level full factorial design was used,
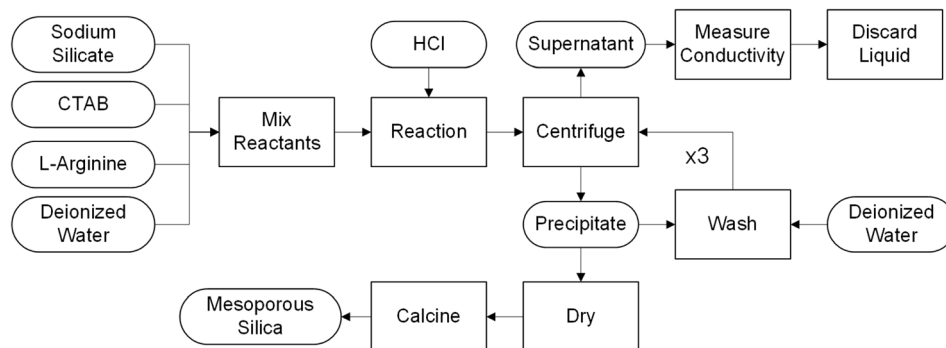
This journal is © The Royal Society of Chemistry 2025

J. Mater. Chem. A, 2025, **13**, 37044–37062 | **37045**

Fig. 1 Flow diagram showing the typical procedure used for the synthesis of mesoporous silica with bio-inspired additives.

meaning that for each factor, two-levels are explored, and every combination of these factors is tested. Compared with an experimental design that modifies one factor at a time, this design has the advantage of being able to identify the effects of changing combinations of factors.[24]

From prior work with bio-inspired silica[3] and surfactant-templated silica materials,[25] four factors were initially identified as having potential importance in the synthesis system, giving 16 synthesis conditions in total for the initial two-level four-factor experimental design: concentration of the silica precursor ([Si]), silicon to amine molar ratio (Si : N), silicon to CTAB molar ratio (Si : CTAB), and final reaction pH. The silicon to amine ratio (Si : N) refers to the molar ratio of silicon atoms in silicates to amine groups in the bio-inspired additive, which has been shown to be important in directing bio-inspired silica synthesis,[3,4] and does not include the nitrogen in the ammonium group present in CTAB molecules. The final reaction pH refers to the pH following the addition of hydrochloric acid, which induces the precipitation of silica. The levels used in the two-level four-factor experiment design are given in Table 1 (Samples 1–1 through 1–16). These are compared with three samples from literature, the synthesis conditions of which are labelled A, B and C in Table 1. The first sample (A) chosen for comparison is the initial synthesis of MCM-41 by Beck *et al.* In this synthesis, a relatively high surfactant concentration was used (25 wt%) and hydrothermal treatment was carried out at 100 °C for 144 hours.[5] The second sample (B) is a synthesis of well-ordered MCM-41 at room temperature using a low surfactant concentration, presented by Cai *et al.* This synthesis used TEOS as a silica precursor, and ammonia was used to control the synthesis pH. A minimum reaction time of 2 hours was used in this synthesis.[14] The third sample (C) is a synthesis of MCM-41 from sodium silicate. This synthesis used the same silica to surfactant ratio as Cai *et al.* but did not obtain very well ordered materials except after hydrothermal treatment was used, as indicated by reported XRD patterns. The sample chosen for comparison was the one synthesised at room temperature without hydrothermal treatment.[15]

After the initial two-level four-factor study, further experiments were carried out to look in more detail at the responses of modifying particular factors on material properties. Full details of these experiments are also given in Table 1, including the

effect of modifying the component ratios, Si : N and Si : CTAB (Samples 2–1 through 2–6); the effect of using alternative bio-inspired additives (Samples 3–1 through 3–5); the effect of modifying Si : N ratio and reaction time (t_{rxn}) for a system with pentaethylenehexamine (Sigma-Aldrich technical grade) instead of arginine (Samples 4–1 through 4–7). Full results of this extensive experimental campaign are provided in ESI (Section S.1),† while selected results and trends are discussed in the main body of the paper.

2.3 Sample analysis

After the synthesis was carried out following the procedure in Section 2.1, critical responses were measured. The critical responses identified and the analysis techniques used to quantify them are summarised in Table 2. To identify whether any responses to changes in synthesis conditions were statistically significant, uncertainties were estimated based on repeat samples synthesised under the same conditions (see ESI Section S.2† for details).

The yield of silica is defined as the percentage of silica precursor that is converted into mesoporous silica product. Since the initial concentration of silicon is known, the yield can be calculated from the final mass of silica after calcination:

$$\text{Yield}(\%) = \frac{\left(\frac{m_{SiO_2}}{M_{SiO_2}}\right)}{C_{Si} V} \times 100 \qquad (1)$$

where m_{SiO_2} is the mass of dried silica after calcination, M_{SiO_2} is the molecular weight of silica (60.02 g mol⁻¹), C_{Si} is the concentration of silicates in the reaction mixture and V is the reaction volume. It is assumed that dried samples contain no water after 48 hours of drying at 60 °C, so the dried weight includes only precipitated silica, the bound surfactant template and any additive embedded within this structure. Since these species are completely removed by the calcination step, the organics content of the precipitate before calcination can be calculated.

N₂ adsorption measurements (at 77 K) were taken using the Micromeritics Tristar II 3020. BET surface area was determined using the Brunauer–Emmett–Teller (BET) method[26] and following the procedure of Rouquerol *et al.* to improve consistency in surface area determination.[27] The pore size distribution

37046 | *J. Mater. Chem. A*, 2025, **13**, 37044–37062

This journal is © The Royal Society of Chemistry 2025

Table 1 Input parameters for synthesis of bio-inspired ordered mesoporous silica. The conditions of selected syntheses from literature (labelled A–C) are also included for comparison

Sample no.	[Si] (mM)	Additive	N per additive	Si : N	Si : CTAB	pH	t_{rxn} (min)
A[5]	800	None	—	—	0.87	> 13	2880
B[14]	106	Ammonia	1	0.014	8	11.4	120
C[15]	106	None	—	—	8	11	120
Preliminary	100	Arginine	4	2	2	10	5
1–1	24	Arginine	4	0.10	0.40	7	5
1–2	112	Arginine	4	0.22	0.28	7	5
1–3	24	Arginine	4	0.10	4.00	7	5
1–4	112	Arginine	4	0.22	4.08	7	5
1–5	27	Arginine	4	5.00	0.45	7	5
1–6	128	Arginine	4	5.00	0.32	7	5
1–7	27	Arginine	4	5.00	4.50	7	5
1–8	126	Arginine	4	5.00	4.59	7	5
1–9	27	Arginine	4	0.10	0.45	10	5
1–10	100	Arginine	4	0.20	0.25	10	5
1–11	27	Arginine	4	0.10	4.50	10	5
1–12	112	Arginine	4	0.20	4.08	10	5
1–13	27	Arginine	4	5.00	0.45	10	5
1–14	120	Arginine	4	5.00	0.30	10	5
1–15	27	Arginine	4	5.00	4.50	10	5
1–16	126	Arginine	4	5.00	4.59	10	5
2–1	100	Arginine	4	2	2	10	5
2–2	100	Arginine	4	2	8	10	5
2–3	100	Arginine	4	2	16	10	5
2–4	100	Arginine	4	16	2	10	5
2–5	100	Arginine	4	16	8	10	5
2–6	100	Arginine	4	16	16	10	5
3–1	100	Arginine	4	2	2	10	5
3–2	100	Ammonia	1	2	2	10	5
3–3	100	PEHA	6	2	2	10	5
3–4	100	Propylamine	1	2	2	10	5
3–5	100	None	—	—	2	10	5
4–1	100	PEHA	6	0.333	8	10	5
4–2	100	PEHA	6	0.083	8	10	5
4–3	100	PEHA	6	0.056	8	10	5
4–4	100	None	—	—	8	10	5
4–5	100	PEHA	6	0.333	8	10	60
4–6	100	PEHA	6	0.083	8	10	60
4–7	100	None	—	—	8	10	60

was determined through the Barrett–Joyner–Halenda[28] method from desorption data, which can be used to determine total pore volume within a particular range of pore sizes in the mesoporous region. Pore volumes (V_{pore}) reported in this work were calculated by taking the cumulative pore volume between 1 and 10 nm as determined by BJH desorption. The average pore size (d_{pore}) was determined from the location of the primary peak of the pore size distribution.

Diffraction data was obtained using the Panalytical X'Pert[3] X-ray diffraction (XRD) system. The d_{100} spacing, which relates to

Table 2 Measured responses to two-level four-factor experimental design and their respective analytical technique

Response	Variable	Unit	Uncertainty	Analysis technique(s)
Yield	Y	%	10	Weighing after calcination
Organic content	—	%	5	Weight loss after calcination
BET surface area	S_{BET}	$m^2\ g^{-1}$	70	N_2 adsorption (BET)
Pore size distribution	—	—	0.06	N_2 adsorption (BJH desorption)
Pore volume	V_{pore}	$cm^3\ g^{-1}$	0.1	N_2 adsorption (BJH desorption)
Pore size	d_{pore}	nm	0.1	N_2 adsorption (BJH desorption)
Diffraction pattern	—	—	—	XRD
d_{100} spacing	d_{100}	nm	—	XRD
Pore wall thickness	th_{wall}	nm	0.1	XRD/N_2 adsorption (BJH desorption)
Order parameter	I_{200}/I_{110}	—	0.1	XRD

This journal is © The Royal Society of Chemistry 2025

J. Mater. Chem. A, 2025, **13**, 37044–37062 | **37047**

the inter-pore distance (a_0) for hexagonally ordered pores, can be determined from the location of the first XRD peak using Bragg's equation. a_0 can be determined from d_{100} for a hexagonal lattice:

$$a_0 = \frac{2d_{100}}{\sqrt{3}} \qquad (2)$$

The inter-pore distance can also be used in conjunction with the pore size (d_{pore}) to estimate the pore wall thickness (th$_{wall}$).

$$\text{th}_{wall} = a_0 - d_{pore} \qquad (3)$$

In order to quantify the degree of structural ordering present in samples, an order parameter is devised based on the relative XRD intensity of reflection lines (200) and (110). This procedure was previously used by Cai *et al.* in the characterisation of MCM-41 materials.[14] A ratio closer to 1 indicates a higher level of structural ordering as there is a proportional relationship between the two directions of the crystal structure. Where no peak at reflection line (200) is detectable by the software but a peak exists at reflection line (110), the order parameter I_{200}/I_{110} is considered to be 0, indicating a very low level of hexagonal ordering. To determine the order parameter I_{200}/I_{110} from literature data, the intensity of peaks I_{200} and I_{110} were measured graphically and the baseline reflection was subtracted (see ESI Section S.3†).

2.4 Simulation details

All computational work was carried out using the GROMACS 2022.1 software package, which allows molecular dynamics (MD) simulations to be carried out with high computational efficiency due to the use of state-of-the-art algorithmic optimizations and parallelization.[29,30] For analysis of simulation data, the built-in GROMACS analysis tools were used, as well as the MDAnalysis library for Python.[31,32] Graphs were generated using the Matplotlib library for Python.[33]

Arginine and PEHA atomistic simulations were used to determine bonded parameters for the coarse-grained (CG) model. In both cases, an atomistic model corresponding to an overall neutral molecular charge was used, removing the need to include counter-ions in these simulations. The parameters for arginine were taken from the OPLS model,[34] with the charge of the alpha carbon reduced by 0.02 in order to achieve a neutral overall charge for the molecule. The atomistic model for PEHA was generated using the LigParGen OPLS/CM1A parameter generator utility with localised bond-charge corrected CM1A charges.[35–37] The rigid single point charge (SPC/E) potential was chosen to represent water molecules.[38] The combination of OPLS and SPC/E atomistic force fields was previously used by our group and shown to describe well the self-assembly of ammonium surfactants in aqueous solutions, with and without the presence of silica.[39–41] In these atomistic simulations, a single additive molecule was placed in a cubic box with a side length of 3 nm and periodic boundary conditions. The box was then solvated with an appropriate number of water molecules to achieve a realistic density using the gmx solvate tool in

GROMACS. The leapfrog algorithm[42] was used with a time step of 2 fs. All simulations took place at room temperature (298 K) and pressure (1 bar) using the velocity-rescaling thermostat[43] and the Parrinello–Rahman barostat.[44,45] A 1.2 nm cut-off was used for Lennard-Jones (LJ) interactions with a switching function between 0.9 and 1.2 nm. Long range dispersion corrections for both energy and pressure were applied. Electrostatic interactions were accounted for by the particle-mesh Ewald method.[46,47] Before MD for all atomistic simulations, energy minimisation was carried out using the steepest descent algorithm followed by equilibration in the NVT and NpT ensemble consecutively for 100 ps each, and a production run of 50 ns. Bonded parameters were generated from simulation trajectories using the PyCGTOOL utility.[48]

In order to better understand the experimental findings, coarse-grained MD was used to study the formation of the silica/surfactant mesophase under different conditions. This self-assembly occurs in solution during the early stages of OMS synthesis (*i.e.* before addition of acid), at high pH (≥13). The CG models for silicates and CTAB, consistent with the Martini 3 framework,[49] were developed and validated in a previous publication.[50] Since models compatible with Martini 3 are not available for the bio-inspired additives L-arginine and PEHA at high pH, where self-assembly takes place, these were developed in this work (see ESI Section S.4† for details). After setting up the initial configuration, energy minimisation was carried out using the steepest-descent algorithm. NVT equilibration was carried out using a velocity-rescaling thermostat[43] with a 2 fs time step. NpT equilibration was carried out using the C-rescale barostat,[43] also with a 2 fs time step. Production MD runs used a timestep of 30 fs unless otherwise stated, using the leap-frog algorithm. For temperature control, a velocity-rescaling thermostat was used and the pressure was controlled with the Parrinello–Rahman barostat.[44,45] A different barostat was used for equilibration and production MD because the Parrinello–Rahman barostat is prone to oscillating behaviour during equilibration. For Lennard-Jones terms, the Verlet cutoff scheme[51] was used with a cutoff value of 1.1 nm. Electrostatics were accounted for using reaction field with a cutoff value of 1.1 nm and a relative permittivity of $\varepsilon_r = 15$.

The effect of Si:CTAB ratio and pH on self-assembly was studied initially, as these factors were identified as having the greatest impact on the degree of order of the materials that were synthesised experimentally. For these simulations, arginine was neglected for simplicity. Self-assembly simulations were carried out at Si:CTAB ratios between 0.5 and 16 and pH values of 7, 10 and 13. A "slab" shaped rectangular box arrangement was adopted with a single short dimension (L_z) and two longer box dimensions (L_x and L_y). This short dimension allows for phase separation to occur while using fewer surfactant molecules and thus limiting the overall size of simulations, preventing them from becoming too computationally demanding. A fixed number of surfactant molecules are used for each simulation ($N_{CTAB} = 1000$) and the total number of silicon atoms are set to achieve the desired Si:CTAB ratio. The speciation of silica species represents an experimentally realistic population at pH 13, based on the work of Firouzi *et al.*,[52] of 25% monomers and

37048 | *J. Mater. Chem. A*, 2025, **13**, 37044–37062

This journal is © The Royal Society of Chemistry 2025

Table 3 Population of charge states for silica octamers and monomers used in simulations to represent different system pH

pH	% octamer charge					% monomer charge	
	0	−1	−2	−3	−4	0	−1
13	0	0	0	50	50	0	100
10	0	26	74	0	0	76	24
7	87	13	0	0	0	100	0

75% cubic octamers. The charge of silica species is calculated based on system pH following the method described in ESI (Section S.5).† Charged states with a low proportion of species (less than 5%) are disregarded and the total population is adjusted proportionally. The populations of charged silica species used in these simulations are summarised in Table 3. For Si : CTAB ratios between 2 and 16, the number of water molecules is adjusted to achieve a constant concentration of silica species. For Si : CTAB ratios of 0.5 to 1, a silica concentration 4 times lower is used in order to prevent the simulation volume from becoming too small, leading to low values of box dimensions x and y and allowing bridging of the concentrated surfactant phase across these dimensions. However, this lower silica concentration is not expected to affect self-assembly behaviour, as at low Si : CTAB ratios the silicate species become concentrated in the surfactant rich region of the simulation box, regardless of the bulk concentration of silica. In order to speed up phase separation and equilibration of the system, the initial configuration concentrates all surfactant species within one area of the simulation box while other species are randomly distributed throughout the entire box. After initial equilibration, calculations are carried out for 3 μs of simulation time.

Self-assembly simulations were also carried out in the presence of the bio-inspired additives. For these simulations, only anionic silica dimers were used, as these have been shown to be sufficient to permit the formation of the hexagonal liquid crystal phase,[20] and the interactions of the additives with the silica/surfactant interface are not expected to be significantly different when a more realistic population of silica species (i.e. cubic octamers and monomers) is used. These simulations started from a random configuration of CTAB, L-arginine/PEHA and silica dimers in water, using an elongated simulation box to speed up phase separation and the formation of a HLC phase as in the work of Pérez-Sánchez et al.[20] Full simulation details are given in ESI (Section S.6).†

3 Results & discussion

The characterisation results for a material synthesised following the method described in Section 2.1 using arginine as an additive are shown in Fig. 2. The conditions for this synthesis were; [Si] = 100 mM, [Si : N] = 2, Si : CTAB = 2, pH = 10, t_{rxn} = 5 min. The TEM imaging shows that particles are hexagonally ordered, and this is supported by XRD, which shows three well-resolved peaks (100), (110) and (200) that indicate a hexagonal arrangement of pores. The sample possesses a high BET surface area of 1149 m² g⁻¹ and pore volume of 0.789 cm³ g⁻¹. The pore size distribution is relatively narrow with a mean pore diameter of 2.18 nm.

To investigate the effect of the multiple synthesis parameters in more detail, we carried out an initial two-level four-factor experimental design, the conditions of which are shown in Table 1 (Samples 1–1 through 1–16). A plot showing the parameter space covered by this design is shown in Fig. 3, together with the parameters of the preliminary experiment. Each factor has two-levels, one low and one high value, and expands the parameter space from the original sample in all directions. We now examine the effect of each synthesis parameter separately.
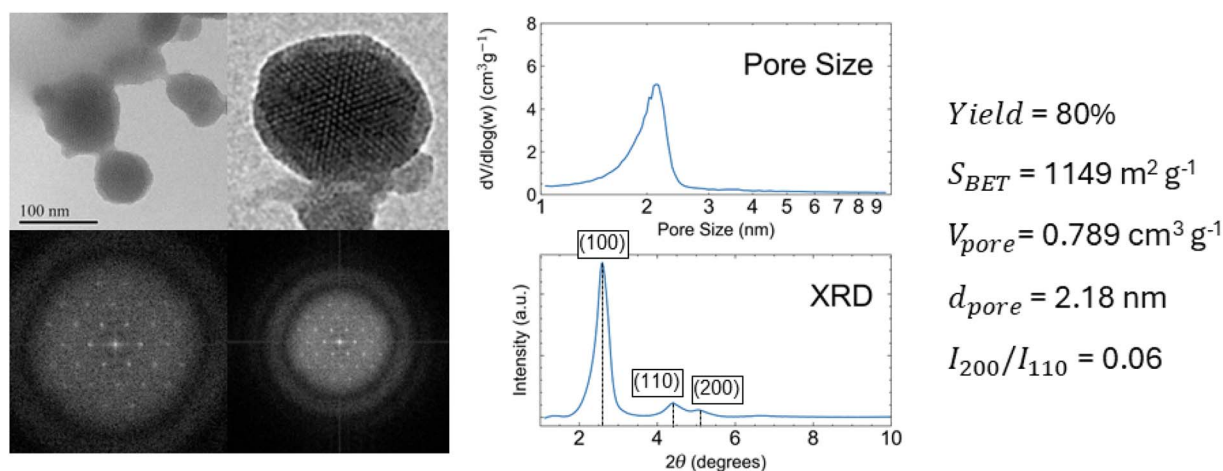

$Yield = 80\%$

$S_{BET} = 1149 \text{ m}^2 \text{ g}^{-1}$

$V_{pore} = 0.789 \text{ cm}^3 \text{ g}^{-1}$

$d_{pore} = 2.18 \text{ nm}$

$I_{200}/I_{110} = 0.06$

Fig. 2 Characterization results for representative OMS samples produced using our synthesis method. TEM imaging is shown on the left, BJH pore size distribution (top) and XRD reflection patterns (bottom) are shown in the middle, and a summary of the yield, BET surface area, pore volume, mean pore diameter and order parameter I_{200}/I_{110} is shown on the right. On the XRD graph, the reflection lines (100), (110) and (200) are labelled. TEM images shown are for the preliminary sample while the remainder of the results are for Sample 3–1, which was synthesised under the same conditions.

This journal is © The Royal Society of Chemistry 2025

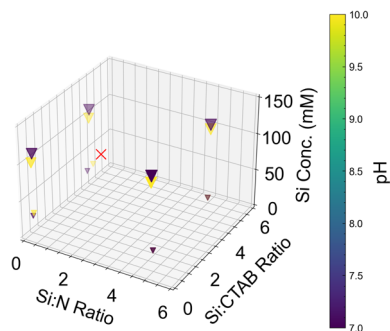J. Mater. Chem. A, 2025, **13**, 37044–37062 | **37049**

Fig. 3 Parameter space covered by the two-level four-factor experimental design detailed in Table 1. The preliminary experiment is shown as a red cross. Symbol size is proportional to silicate concentration.

Fig. 4 Dependence of yield on silica concentration and pH for all samples produced in the two-level four-factor factorial design.

3.1 Silica precursor concentration and final synthesis pH

Although not commonly reported in OMS synthesis studies, the yield is a crucial variable for scale-up, strongly influencing the economic viability of the material manufacturing process. Yield results for the screening experiments are summarized in Table 4, while Fig. 4 shows the dependence of yield on both silica concentration and pH (notice that, as explained in Section 2.1, this is the final synthesis pH). At low silica precursor concentration (<30 mM), the yield of all samples synthesised at pH 10 is consistently higher than samples synthesised at pH 7. At high silica precursor concentration (>100 mM) samples showed much higher yields than low concentration samples, and the dependence on pH was no longer observed. A majority of samples produced at the higher silica precursor concentrations showed high yields of over 75%, suggesting that a large amount of silica precursor present in the system is precipitated in the solid product. The Si : N ratio and Si : CTAB ratio did not appear to have any strong influence on yield.

These results clearly suggest that a higher silica concentration is favourable to improve the overall yield of the synthesis, which may be explained by faster reaction kinetics due to the increased concentration of silicate oligomers. The reduced yield at low silica concentration and pH 7 can be explained by the fact that the proportion of charged silicates will be much lower at
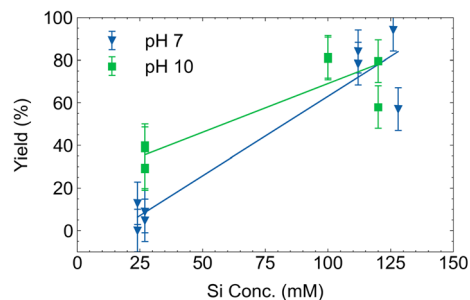
pH 7 than pH 10, with a significant proportion of silicates being present as uncharged molecules.[53] These neutral silicate species will react to form small colloidal silica particles rather than being attracted to the surfactant mesophase.[54] These colloidal particles, which remain suspended, are then lost during centrifugation as they cannot be easily separated from water. At pH 10, a higher proportion of the silicate oligomers are charged and therefore are strongly attracted to the surfactant interface, which improves yield. This effect is reduced at higher silica concentrations, possibly due to the abundance of silicate species which could favour the Ostwald ripening process, causing small silica particles to dissolve and provide material for the growth of larger MCM-41 particles.

A summary of the porosity data is also shown in Table 4, while the corresponding adsorption isotherms, pore size distributions (PSD) and X-ray diffraction (XRD) spectra for each sample are provided in ESI (Fig. S16 and S20).† Note that samples synthesised at low concentration are not included because the sample mass obtained was too low for reliable characterisation by N_2 adsorption and XRD. Since the focus of this investigation was to identify possible "green" synthesis routes for OMS, the samples synthesised at low silica concentration are not of particular interest due to their low yield, and were disregarded from further discussion.

According to the extended IUPAC classifications,[56] all samples with the exception of Samples 1–12 and 1–16 exhibit Type IV(a) behaviour (Fig. S16†): mono and multilayer

Table 4 Summary of yield and porosity data for two-level four-factor screening samples that were characterized by N_2 adsorption and XRD. The variables are fully described in Section 2.3. Comparison is made to available material properties for MCM-41 samples from literature (Samples A, B and C)

Sample no.	Yield (%)	S_{BET} (m² g⁻¹)	V_{pore} (cm³ g⁻¹)	d_{pore} (nm)	d_{100} (nm)	a_0 (nm)	th_{wall} (nm)	I_{200}/I_{110}
A[5,55]	—	1040	0.79	4.00	3.98	4.60	0.60	0.62
B[14]	—	—	—	—	3.48	4.02	—	0.65
C[15]	—	1312	0.86	3.14	3.05	3.52	0.38	0.00
1–2	78	1120	0.906	2.48	4.03	4.65	2.17	0.00
1–4	84	1005	0.828	2.45	3.88	4.48	2.03	0.28
1–6	57	970	0.721	2.51	3.98	4.60	2.09	0.00
1–8	94	1030	0.839	2.30	3.81	4.40	2.10	0.27
1–10	82	1181	0.966	2.63	3.80	4.39	1.76	0.00
1–12	81	1259	0.834	2.12	3.50	4.04	1.92	0.06
1–14	80	1217	1.003	2.55	3.82	4.41	1.86	0.04
1–16	58	1210	0.850	2.14	3.68	4.25	2.11	0.08

37050 | J. Mater. Chem. A, 2025, 13, 37044–37062

This journal is © The Royal Society of Chemistry 2025

adsorption plus capillary condensation,[57] which is typical of mesoporous materials,[58] with a hysteresis loop indicating irreversible adsorption. However, the hysteresis effect is not strong, indicating small mesopores close to or below the critical width (<4 nm). Samples 1–12 and 1–16 show Type IV(b) isotherms, indicating mesopores with dimensions much smaller than the critical width. The average pore sizes, d_{pore}, which are also reported in Table 4, confirm these observations. Most PSDs (Fig. S20†) show a relatively narrow peak centered around 2–2.5 nm, indicating that those samples contain mesopores with a regular size.

The BET surface area for all samples was high (>970 m² g⁻¹) indicating a high level of porosity. This is comparable to the value of 1070 m² g⁻¹ reported in the initial discovery of MCM-41, which was synthesised with a hydrothermal treatment step.[5] Surface area was most strongly dependent on synthesis pH, with samples synthesised at pH 10 having a surface area that was, on average, 186 m² g⁻¹ greater than samples synthesised at pH 7 (see Fig. 5), which is statistically significant. While the pore volume also seems to be slightly higher at pH 10, this is within the estimated statistical uncertainty (Fig. S35†).

All samples showed a well-resolved XRD peak at approximately $2\theta = 2°$ (Fig. S20†), corresponding to the reflection line (100) and indicating the presence of an ordered hexagonal structure. Two further peaks can be seen between $2\theta = 4–5°$ which correspond to the reflection lines (110) and (200). The intensity of these lines indicates a well-ordered hexagonal pore geometry for these materials.[59] All samples possess a discernible peak at reflection line (110), however only five of the samples (Samples 1–4, 1–8, 1–12, 1–14 and 1–16) possess a clear peak corresponding to reflection line (200). This suggests that the degree of structural ordering of the remaining samples (Samples 1–2, 1–6 and 1–10) is poor. This finding is in agreement with the pore size distributions generated from N₂ adsorption isotherms (Fig. S20†), suggesting that a high Si : CTAB ratio promotes the formation of a more well-ordered hexagonal structure than when a low Si : CTAB ratio is used. The samples synthesised using both a high Si : CTAB ratio and a pH of 7 had the highest order parameter by a significant margin. This may be attributed to the faster reaction rate of silica condensation reactions at pH 7 *versus* pH 10, which allows the hexagonal mesophase formed at high pH to become "locked in" as suggested by computational studies of mesoporous silica

synthesis,[18] a point to which we will return later in this paper. It also indicates that, while samples synthesised at both pH values have comparable pore size distributions, the samples synthesised at pH 7 possess a higher degree of order despite having lower surface area and pore volumes, suggesting that there is a trade-off between achieving high surface area and a high degree of order, and that the surface area of the material is not strongly dependent on the level of ordering of pores.

The material properties of samples obtained by this synthesis procedure are compared with selected MCM-41 samples from literature (Samples A, B and C in Table 4). Note that no gas adsorption data was provided by Cai *et al.* (Sample B), preventing comparison of some material properties. Materials synthesised in this work showed similar BET surface areas and pore volumes when compared to samples A and C. The pore diameters of samples synthesised in this work are smaller than reported in samples A and C, while the pore wall thickness is much larger. Thick pore walls were also observed in the work of Lin *et al.*,[13] which was attributed to the "delayed neutralization" procedure, in which the self-assembly of the material takes place at high pH, prior to addition of an acid, which brings the pH to a value in which silica condensation takes place. However, Lin *et al.* did not observe ordered materials at reaction times of 30 minutes, with samples requiring several days of ageing in order to achieve well-resolved XRD peaks indicating hexagonal ordering. The reason that ordered materials were obtained without ageing in this work may be due to the rapid addition of acid, which is added in a single step rather than being added slowly. This rapid addition of acid may allow the highly ordered structure to be more effectively locked in before disorganisation of the mesophase can occur.

The largest difference from literature samples is observed in the order parameter I_{200}/I_{110}. All samples synthesised in this two-level four-factor screening possess a lower order parameter than sample A, which was synthesised using hydrothermal treatment. However, two of the samples synthesised by this method, samples 1–4 and 1–8, possess significantly higher order parameters than sample C, which was synthesised from sodium silicate without hydrothermal treatment. This demonstrates that a high level of structural ordering can be obtained without the need for hydrothermal treatment by modification of the synthesis method. The key difference is that the reaction pH is achieved by first obtaining a high pH mixture, and then rapidly adding acid to induce precipitation of the porous silica mixture. As discussed by Lin *et al.*,[13] this pH control method helps to maintain the well-ordered structure that forms at high pH throughout the synthesis step. Sample B, which was synthesised at room temperature using a low surfactant concentration, has a higher degree of order than the samples obtained in our DoE study. However, this was achieved through manipulation of the Si : CTAB ratio, which is investigated further in Section 3.3. Sample B also had a significantly longer reaction time of 2 hours, while the samples presented here were precipitated in just 5 minutes. None of the literature synthesis studies compared here presented yield values, which are rarely reported in material synthesis despite being critical for scale-up.
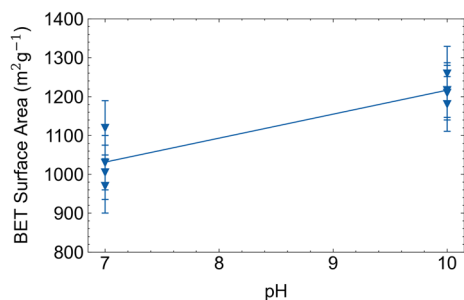

Fig. 5 Dependence of BET surface area on pH. The line is a guide to the eye.

This journal is © The Royal Society of Chemistry 2025

J. Mater. Chem. A, 2025, **13**, 37044–37062 | **37051**

Table 5 Summary of yield and porosity data for component ratio investigation samples that were characterized by N_2 adsorption and XRD. The variables are fully described in Section 2.3

Sample no.	Yield (%)	S_{BET} (m² g⁻¹)	V_{pore} (cm³ g⁻¹)	d_{pore} (nm)	th_{wall} (nm)	I_{200}/I_{110}
2–1	87	1259	0.971	2.31	1.80	0.12
2–2	47	1165	0.841	2.15	1.78	0.46
2–3	16	1159	0.843	2.13	1.84	0.00
2–4	91	1193	0.857	2.22	1.84	0.11
2–5	39	1144	0.824	2.14	1.82	0.50
2–6	17	1194	0.898	2.25	1.76	0.07

3.2 Si to N ratio

In the two-level four-factor screening investigation, changes in the Si : N ratio, at least within the examined range, did not produce any noticeable changes in the responses examined, either in structural properties or yield. This was somewhat surprising, and casts some doubt on the role of the chosen bio-inspired additive, L-arginine, for promoting the rapid formation of ordered silica materials under ambient conditions. To investigate this further, additional experiments were carried out with different Si : N ratios at the high end of the range, as well as a "control" experiment without any additive – *i.e.* with a Si : N ratio of infinity. The Si : CTAB ratio was also varied in this new set of experiments, in order to study the effect of that parameter in more detail (see Section 3.3). The synthesis procedure is the same as was laid out in Section 2.1, and the silica concentration and synthesis pH were kept fixed at 100 mM and 10, respectively. The synthesis conditions used in this investigation are shown in Table 1 (Samples 2–1 through 2–6).

The yield results and porosity data are summarised in Table 5 (see also ESI, Fig. S17† for the nitrogen adsorption isotherms). The yield seems to be virtually independent of the Si : N ratio, and no strong correlations were found between that factor and BET surface area, pore volume, pore size, d_{100} spacing or wall thickness. This confirms the conclusion of the screening study, and suggests that the presence of L-arginine does not play a major role in controlling the structural properties of the material. More importantly, it also seems to have no effect on the promotion of order within the pore network, as observed by comparing the pore size distributions and XRD spectra (see Fig. 6) for these samples. In fact, it is quite remarkable that the sample synthesised without any bio-inspired additive also produces mesoporous silica with a high degree of order.

In order to understand why L-arginine does not impact the structure of materials formed in this synthesis, a coarse-grained MD simulation of the self-assembly of the silica/surfactant mesophase was carried out with L-arginine present. The final configuration after 6 μs of simulation time is shown in Fig. 7b. The surfactant can clearly be seen to adopt a HLC arrangement identical to the behaviour exhibited in a system containing CTAB and silica dimers where arginine is not present.[20] This suggests that the presence of arginine does not affect the silica-surfactant mesophase formation.

A snapshot of a cross section of the simulation box showing only arginine and surfactant headgroup beads is shown in Fig. 7c. From this snapshot, it is clear that arginine primarily inhabits the bulk water region with only a small number of arginine molecules being present within the surfactant-rich region. This can be attributed to weak interaction of arginine with the silica-surfactant interface. This is further evidenced in Fig. 7d, where the relative density of arginine approximately follows the relative density of water, with high relative density in the bulk water and very low relative density in the surfactant rich region. This may explain why incorporating arginine into OMS synthesis does not affect the properties of the material produced. Since the arginine primarily inhabits the bulk water, it is likely to be excluded from the self-assembled surfactant template. However, given the previous reports on the interfacial interactions and catalytic effects of arginine in silica formation,[3,16,17] results reported herein on the self-assembly do not rule out arginine's potential role in catalysing the early stages of silicic acid condensation. We aim to address this in future work using *in situ* measurements of chemical kinetics coupled with simulations of the reactions using reactive models for silica condensation.[60]

3.3 Silica to surfactant ratio

Contrary to the Si : N ratio, our experiments revealed that the Si : CTAB ratio can have a pronounced effect on at least some material properties. First of all, there is a clear correlation between Si : CTAB ratio and yield, as shown in Fig. 8. While data for low Si : CTAB ratios is rather noisy, it is clear that when Si : CTAB is increased above approximately 4, the yield decreases dramatically, reaching below 20% at a Si : CTAB ratio of 16. As the quantity of surfactant is reduced (increasing Si : CTAB), the amount of surfactant likely becomes insufficient to form large
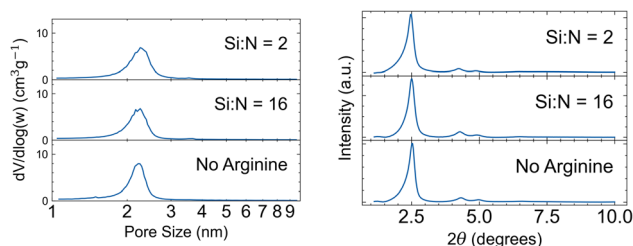

Fig. 6 Pore size distributions (left) and XRD data (right) for selected samples with varying quantities of arginine. For XRD data, baseline intensity was removed manually to allow for easier comparison between peaks.
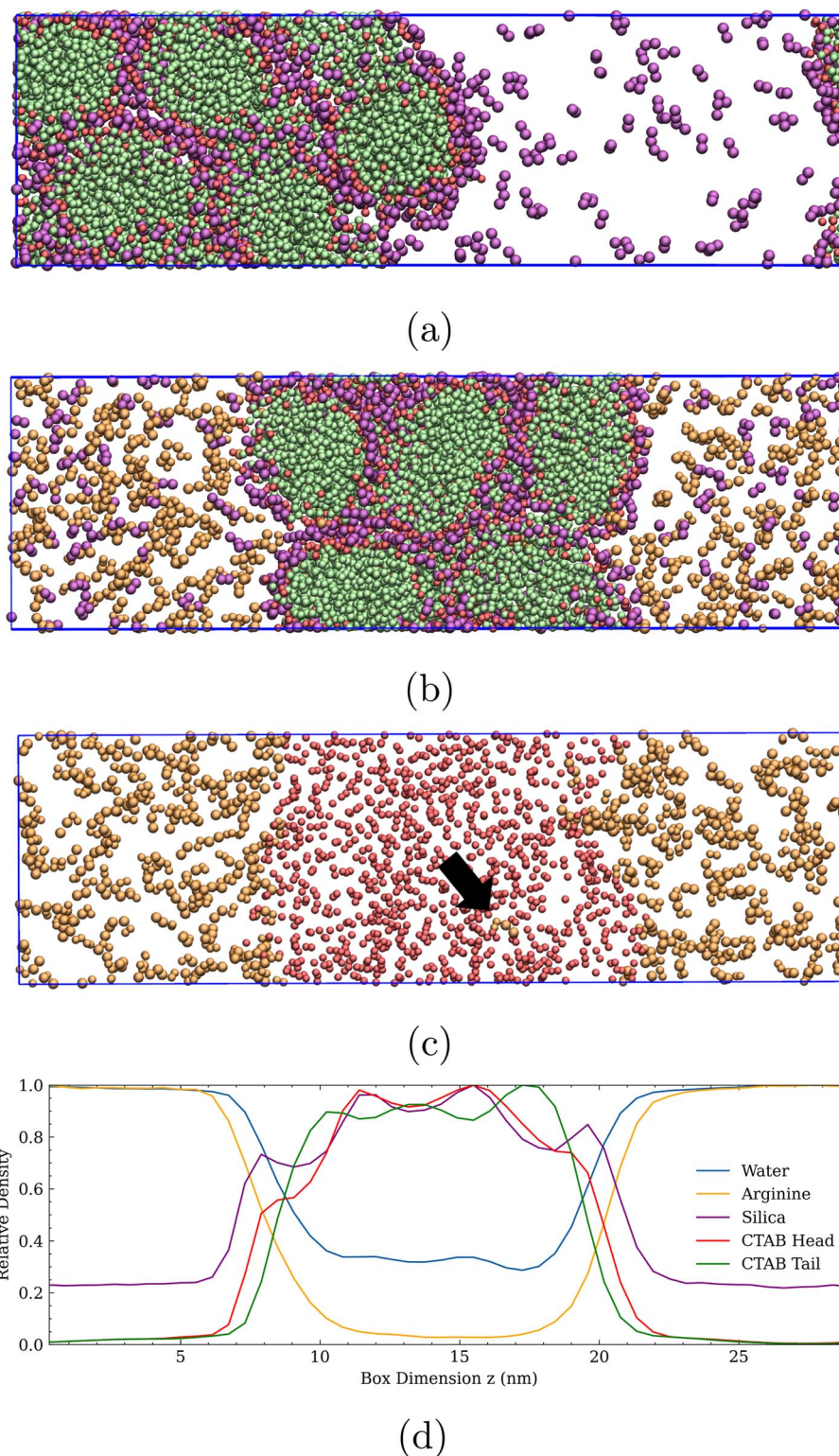
37052 | *J. Mater. Chem. A*, 2025, **13**, 37044–37062

This journal is © The Royal Society of Chemistry 2025

Fig. 7 Snapshots of the final configuration after 6 μs are shown for self-assembly simulations without additive (a) and with arginine ((b) and (c)) starting from a random configuration. CTAB headgroups are shown in red, tails in green, silica dimers in purple and arginine in orange. Water is hidden in all snapshots for clarity. In (d), the time averaged relative densities (calculated as ρ/ρ_{max}) across the z axis for all species are shown. The black arrow in (b) points towards a single arginine case observed in the surfactant phase.

quantities of the product. In fact, the organic content of the silica material also decreases significantly with Si : CTAB (see Fig. S34†). These observations can be explained by the limited quantity of surfactant compared to silicon being ineffective in adequately concentrating silicate species within the surfactant mesophase.

This journal is © The Royal Society of Chemistry 2025

J. Mater. Chem. A, 2025, 13, 37044–37062 | 37053
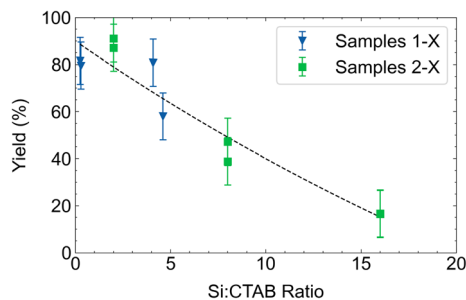
Fig. 8 Dependence of yield on Si : CTAB ratio for samples synthesised at pH 10 with a high silica concentration (>100 mM). Data points for series Samples 1–X correspond to samples 1–10, 1–12, 1–14, and 1–16. The dashed line provides a guide for the eye.

Fig. 10 Dependence of order parameter I_{200}/I_{110} on Si : CTAB ratio for all samples synthesised at a high silica concentration. The dashed line is a guide for the eye.

While there are no strong correlations between Si : CTAB and BET surface area, pore volume, pore size, d_{100} spacing or wall thickness (Table S2†), this factor does seem to affect the degree of order of the pores. For instance, samples synthesised using a Si : CTAB ratio of 8 appear to possess a narrower pore size distribution, more clearly defined XRD peaks (Fig. 9) and a higher I_{200}/I_{110} order parameter (Table S2†). This suggests improved regularity of pores in these samples and a higher degree of structural ordering. However, this does not result in improved bulk characteristics such as increased surface area or total pore volume. In contrast, the resolution of the XRD peaks in samples obtained with a Si : CTAB ratio of 16 is extremely poor and their order parameter is close to zero (Fig. 9). This suggests that these samples possess a very low degree of hexagonal ordering. Examining the order parameter more closely over the whole range of samples synthesised (see Fig. 10), the degree of order appears to be highest in samples synthesised with a Si : CTAB ratio of 8. The degree of order obtained for these samples is similar to the highly ordered MCM-41 samples synthesised by Cai *et al.*, but with a much shorter reaction time.[14] This indicates that the degree of structural ordering of hexagonally arranged pores is improved as the Si : CTAB ratio is increased from 2 to 8, but that this effect is diminished as the ratio is increased further from 8 to 16.

This demonstration of the dependence of both yield and degree of order on Si : CTAB ratio is particularly important, as although previous studies have highlighted the importance of
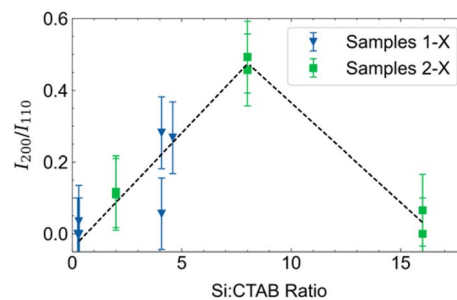
silica to surfactant ratio on material properties,[14,15] most studies do not consider yield. As demonstrated, the optimal conditions for achieving a well-ordered porous structure do not achieve the greatest yield, indicating that a trade off exists that must be considered when attempting to scale-up these synthesis processes.

To understand the effect of the Si : CTAB ratio and pH on the degree of order, coarse-grained MD simulations of self-assembly were carried out under different conditions. Snapshots of the final configurations obtained at varying Si : CTAB ratios are shown in Fig. 11. At pH 13, which represents the system during the early stages of synthesis before the addition of acid, at all Si : CTAB ratios, the presence of silicates is effective in promoting aggregation and phase separation of the surfactant phase. However, the degree of order of this surfactant phase varies with the Si : CTAB ratio. At low Si : CTAB ratios 0.5–2 (Fig. 11a–c) the degree of order is low and (at best) only an incipient HLC phase is observed. However, at a Si : CTAB ratio of 4 (Fig. 11d) a much more well ordered HLC phase is formed. This well-ordered arrangement is preserved at a ratio of 8 (Fig. 11e). At a ratio of 16 (Fig. 11f), the curvature of the surfactant phase appears to increase, resulting in a less well-ordered arrangement.

In Fig. 12, the relative amount of silica that is bound to the surfactant phase is compared with the overall Si : CTAB ratio (*i.e.* in the entire simulation box). The former is calculated by taking an average of the number of silicates that are within 0.73 nm of a surfactant headgroup bead, which corresponds to the first minimum of the surfactant to silica radial distribution function, after the initial equilibration period. The red dashed line indicates where these quantities are equal, *i.e.* all silicon atoms are bound to the surfactant phase. At low Si : CTAB ratios, the data (orange circles in Fig. 12) closely follow this line, indicating that all silica species are bound to the surfactant phase. As the Si : CTAB ratio is increased, the divergence from the ideal line increases, which indicates that as more silicates are added to the system, more remain in solution while the interface becomes saturated. This divergence increases dramatically at a Si : CTAB ratio between 2 and 4, which corresponds to the formation of the HLC phase observed in simulation snapshots (Fig. 11). The bound Si : CTAB ratio then reaches a maximum, at which point further increases in the
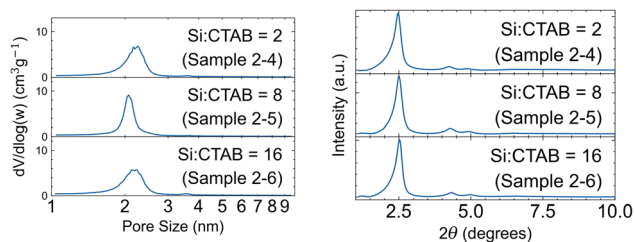

Fig. 9 Pore size distributions (left) and XRD data (right) for selected samples synthesised with different Si : CTAB ratios. For XRD data, baseline intensity was removed manually to allow for easier comparison between peaks.
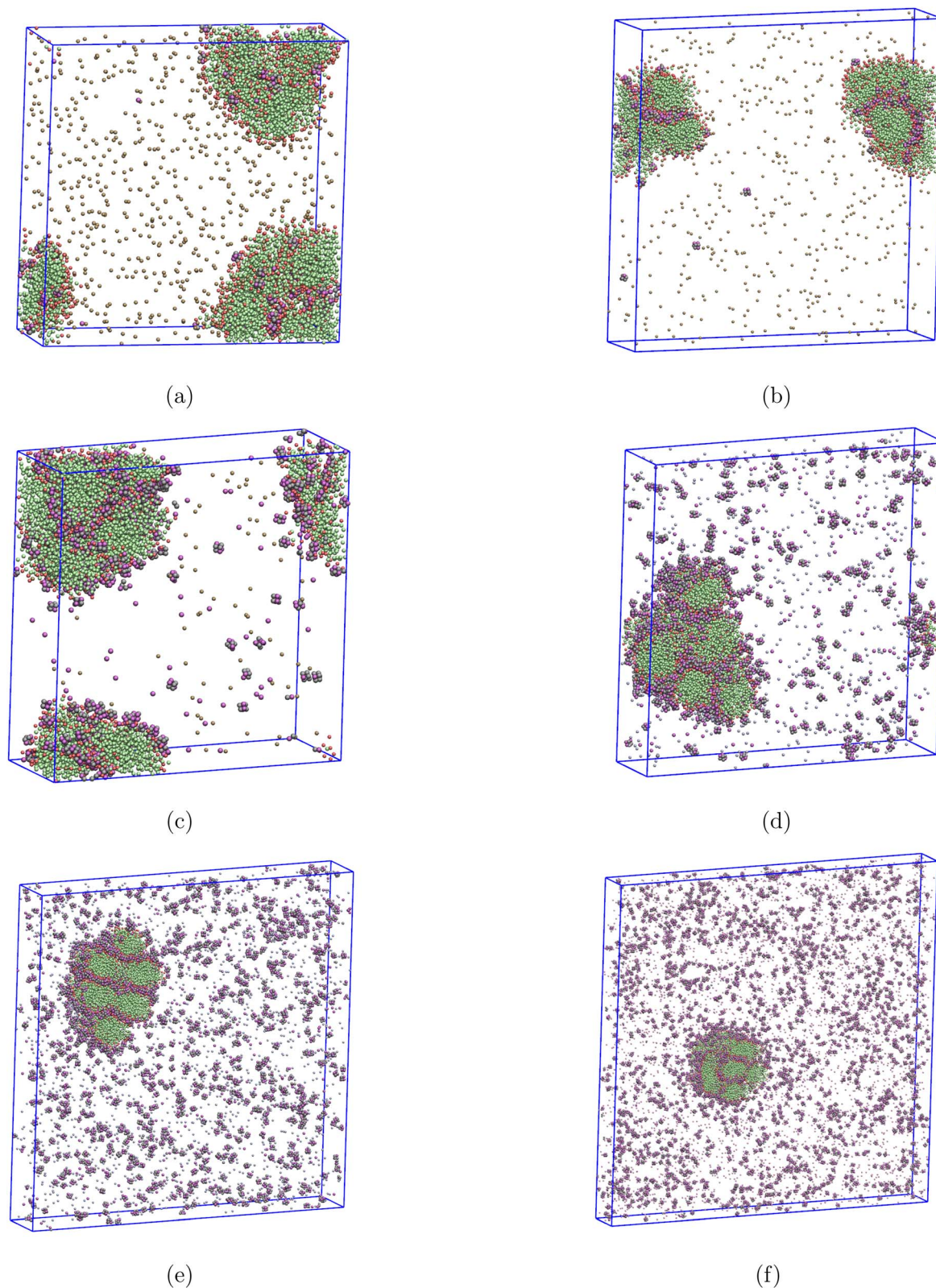
37054 | *J. Mater. Chem. A*, 2025, **13**, 37044–37062

This journal is © The Royal Society of Chemistry 2025

Fig. 11 Snapshots of the final configurations obtained from self-assembly simulations at pH 13 with varying Si : CTAB ratios: (a) = 0.5, (b) = 1, (c) = 2, (d) = 4, (e) = 8, (f) = 16. Full simulation details are given in ESI (Table S8).†

overall Si : CTAB ratio do not increase the bound Si : CTAB ratio, suggesting that the surfactant interface is fully saturated with silicates. This can be explained by considering the overall

charge at the surfactant interface, shown in Fig. 12, which takes into account all charged species that are bound to the surfactant interface, including bromide counter-ions. As the Si : CTAB ratio
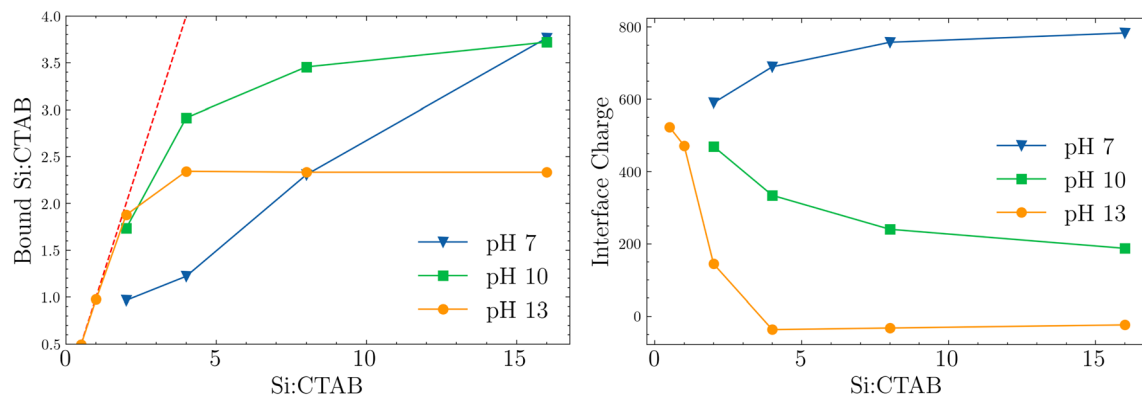
This journal is © The Royal Society of Chemistry 2025

J. Mater. Chem. A, 2025, **13**, 37044–37062 | **37055**

Fig. 12 Effect of varying the Si : CTAB ratio on the quantity of silicon atoms bound to the surfactant phase (left) and the overall charge at the surfactant interface (right) at different pH values, determined from MD simulations. The dashed red line represents an ideal case where all silicon atoms are bound to the surfactant phase.
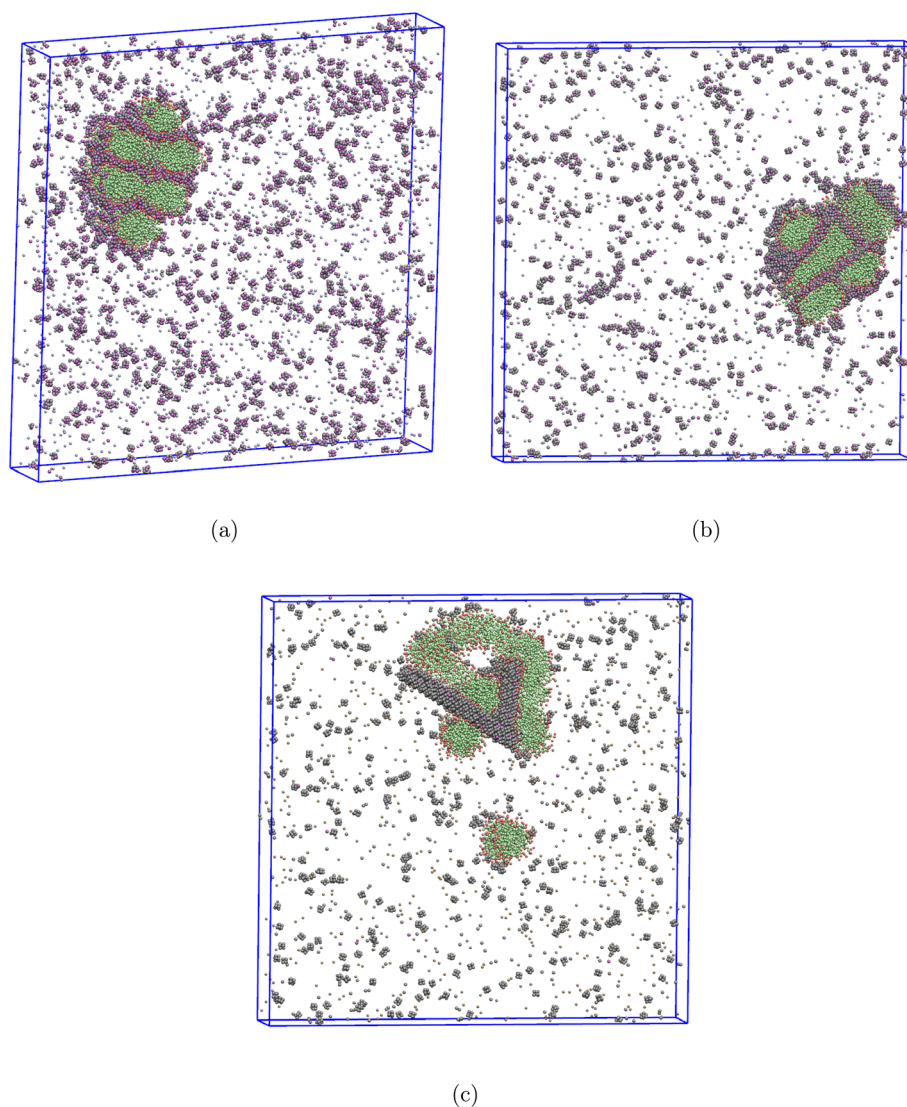

(a)

(b)

(c)

Fig. 13 Snapshots of the final configurations obtained from self-assembly simulations at a Si : CTAB ratio of 8 and at varying system pH: (a) = 13, (b) = 10, (c) = 7. Full simulation details are given in ESI (Table S8).†

37056 | J. Mater. Chem. A, 2025, **13**, 37044–37062

This journal is © The Royal Society of Chemistry 2025

Table 6 Summary of yield and porosity data for additive investigation samples that were characterized by N_2 adsorption and XRD. The variables are fully described in Section 2.3

Additive	Yield (%)	S_{BET} (m^2 g^{-1})	V_{pore} (cm^3 g^{-1})	d_{pore} (nm)	th$_{wall}$ (nm)	I_{200}/I_{110}
L-Arginine	80	1149	0.789	2.18	1.21	0.06
Ammonia	78	1203	0.835	2.17	1.21	0.00
PEHA	74	1218	0.938	2.40	1.23	0.28
Propylamine	65	1273	0.969	2.35	—	0.00
None	81	1218	0.911	2.24	1.26	0.20

is increased, the interface charge, which is initially positive due to excess of cationic surfactant heads, decreases until it becomes approximately neutral. At this point there is no strong driving force for further attraction of silicates to the surfactant interface, as this process is primarily driven by electrostatic interactions between the positively charged surfactant head-groups and the negatively charged anionic silica species. Hence, further addition of silicates past this point does not result in an increase in silica species at the surfactant interface.

Fig. 12 also shows data for bound Si and charge obtained at lower pH values, while Fig. 13 shows snapshots of the final simulation configurations at a Si : CTAB ratio of 8. A hexagonal arrangement is observed at pH 13 (Fig. 13a) as previously discussed. However, at pH 10 (Fig. 13b), while the presence of silica is effective in promoting phase separation, this phase is less well-ordered and appears to have reduced curvature of the silica/surfactant interface forming wider, less cylindrical "pores". As the pH is reduced further to 7 (Fig. 13c), the silicates are less effective at promoting phase separation, with the surfactant instead forming worm-like and spherical micelles. This can be attributed to the much lower proportion of charged silica species present at this pH, which appears to be insufficient to screen the repulsive charge between surfactant micelles, preventing further aggregation of the surfactant phase. This interpretation is confirmed by the data in Fig. 12. At pH 13, the charge at the interface is approximately neutralised at a Si : CTAB ratio of 4, however at pH 10 it is still strongly positive, which may explain the disorder of the phase. While further increases in Si : CTAB ratio appear to reduce the interface charge, the effect is diminished as Si : CTAB ratio is increased, and it is possible that the charge may not be fully neutralised at this pH even at very high

Si : CTAB ratios. The positive charge of this interface allows for more silicates to be attracted to the surfactant phase as the Si : CTAB ratio is increased, as shown in Fig. 12.

The snapshot at pH 7 (Fig. 13c) shows that silicates appear to aggregate into solid clusters due to the lack of charged groups, which would otherwise prevent clustering. This behaviour is not likely to be realistic, as in reality these silica species would undergo condensation reactions to form a more extensive silica network. During the experimental synthesis, these condensation reactions may occur before such extensive rearrangements of the silica/surfactant phase take place, effectively locking in the more well-ordered structure that forms at higher pH. However, since the model used in this work does not allow for silica polymerisation reactions to take place, this process cannot be accurately observed. Since in the experimental synthesis it was observed that hexagonally ordered structures were obtained at both pH 7 and 10, we can conclude that extensive rearrangement of the silica/surfactant phase does not take place upon the reduction in pH, which facilitates silica precipitation. Furthermore, the fact that experimental materials synthesised at pH 7 possess a higher degree of order than the materials synthesised at pH 10 suggests that the faster reaction kinetics of silica condensation reactions at pH 7 allows for the highly ordered structure that forms at high pH (>13) to become locked in more rapidly before rearrangement of the silica/surfactant phase can occur.

3.4 Alternative bio-inspired additives

Since the presence of L-arginine did not appear to affect the assembly of OMS by this method, it was decided to carry out the same synthesis procedure (Section 2.1) using alternative bio-inspired additives. Aside from the additive used, all synthesis conditions were kept the same between samples and are displayed in Table 1 (Samples 3–1 through 3–4). The common feature of all additives in this investigation is the presence of primary or secondary amine groups. The number of these groups present in each additive is also listed in Table 1.

Yield results are shown in Table 6. The yield did not change significantly with the use of different additives, although there was a small decrease in yield when using propylamine. Bulk porosity data is also similar, with all samples exhibiting mesopores of similar size (see Fig. 14) and similar BET surface areas and pore volumes (Table 6). Furthermore, these values are comparable to the sample synthesised without an additive, confirming that the presence of an additive is not essential to obtaining high surface area silica following this synthesis method.
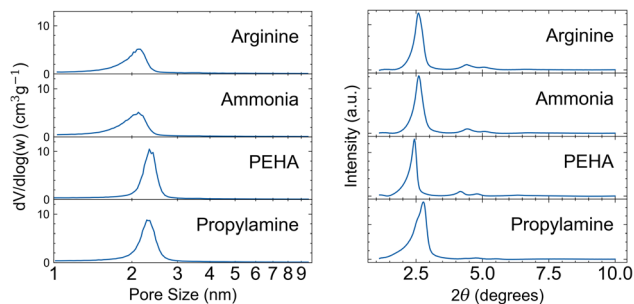

Fig. 14 Pore size distributions (left) and XRD data (right) for selected samples synthesised with different additives. For XRD data, baseline intensity was removed manually to allow for easier comparison between peaks.
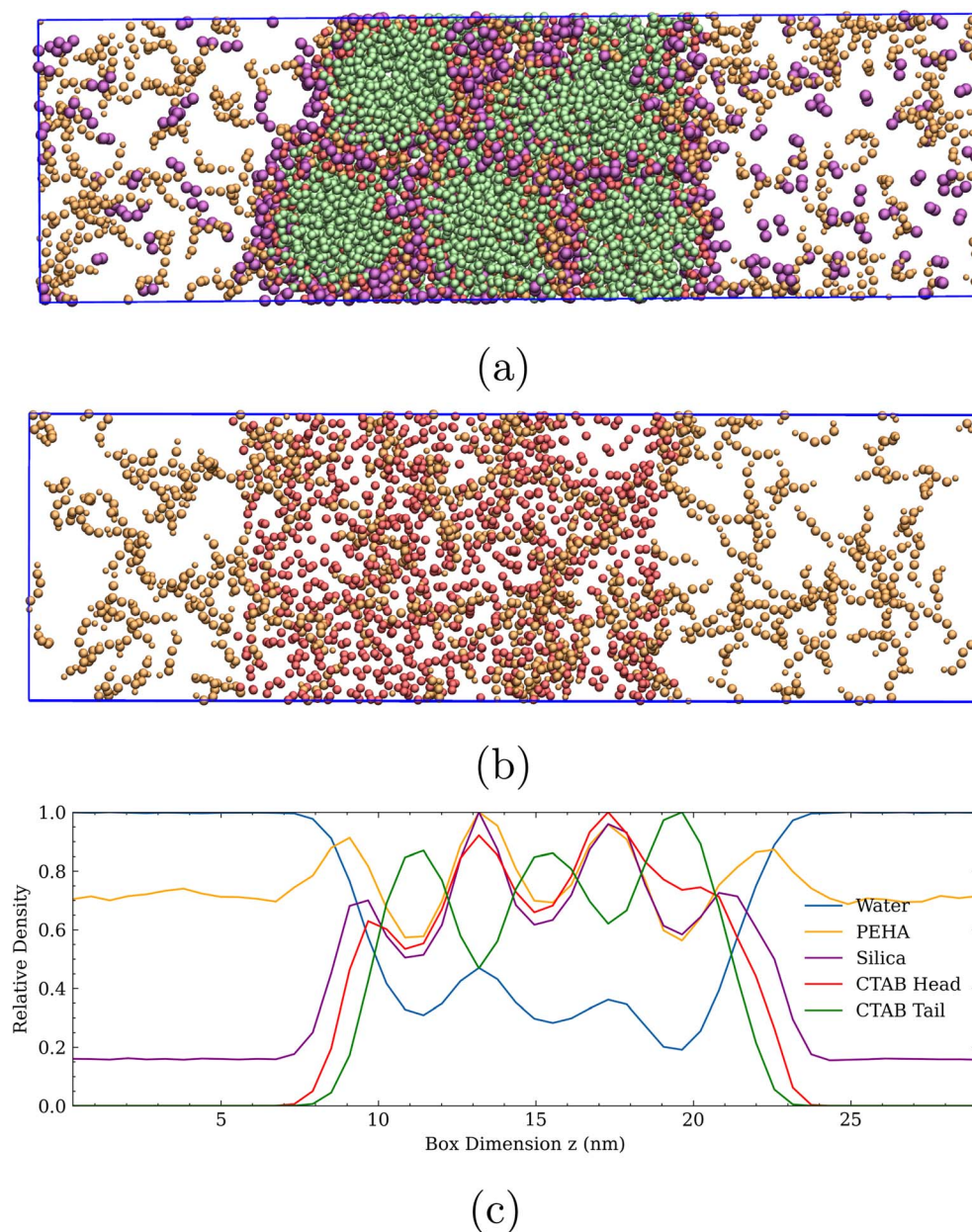
Fig. 15 Simulation snapshots of the final configuration after 6 μs are shown for self-assembly simulations with PEHA ((a) and (b)) starting from a random configuration. CTAB headgroups are shown in red, tails in green, silica dimers in purple and PEHA in orange. Water is hidden in all snapshots for clarity. In (c), the time averaged relative densities (calculated as ρ/ρ_{max}) across the z axis for all species is shown.

A closer look at the pore size distributions (see Fig. 14), however, shows that samples synthesised with L-arginine and ammonia have slightly broader pore size distributions that extend below 2 nm towards the microporous region, whereas the presence of PEHA appears to result in a narrower pore size distribution, suggesting improved structural ordering compared to the other samples. This is confirmed by the XRD results shown in Fig. 14. The sample that was synthesised with PEHA has exceptionally well-resolved reflection lines (100), (110) and (200), and the highest order parameter I_{200}/I_{110} of all samples (Table 6).

To understand why the presence of PEHA was effective in increasing the degree of order of OMS synthesised following this method, a self-assembly simulation was carried out for silica and CTAB in the presence of neutral PEHA molecules, which resembles the system at high pH (pH > 13). The final configuration after 6 μs of simulation time is shown in Fig. 15. The formation of a HLC phase can be observed, indicating that PEHA does not significantly alter mesophase formation at the beginning of the synthesis, while the pH is still high. However, unlike what was previously observed with L-arginine (see Fig. 7), PEHA molecules are present in significant quantities at the silica-surfactant interface, interspersed throughout the HLC phase. This is illustrated in Fig. 15c, which shows that the relative density of PEHA peaks at the same positions as the CTAB headgroup and silica densities. This indicates that at high

Table 7 Summary of yield and porosity data for PEHA investigation samples that were characterized by N_2 adsorption and XRD. The variables are fully described in Section 2.3. Additional data is provided in ESI (Tables S2 and S1)

Sample no.	Yield (%)	S_{BET} ($m^2\ g^{-1}$)	V_{pore} ($cm^3\ g^{-1}$)	d_{pore} (nm)	th_{wall} (nm)	I_{200}/I_{110}
4–1	65	983	0.706	2.20	1.35	0.52
4–2	80	961	0.736	2.27	1.41	0.49
4–3	69	926	0.679	2.24	1.37	0.00
4–4	41	1186	0.830	2.09	1.35	0.18
4–5	78	783	0.608	2.80	—	0.00
4–6	86	878	0.686	2.74	—	0.00
4–7	57	1142	0.841	2.10	1.30	0.29

pH, where the formation of the OMS template takes place, PEHA is incorporated into the framework that will become the porous silica network. Since amine groups (which are numerous in PEHA) are known to catalyse the condensation of silica,[3] this behaviour may provide insight into how the presence of PEHA during synthesis is able to improve the degree of structural ordering in OMS. Incorporation of PEHA species into the HLC may allow it to catalyse the condensation of silica, "locking in" the structure more quickly before it can become disordered due to the drop in quantity of anionic silicates after acid addition.

Given the promising results obtained in the sample with PEHA, we have carried out additional experiments using several ratios of silica to PEHA, with Si : N between 0.333 and 0.056. The Si : CTAB ratio was kept fixed at a value of 8, which was previously identified to produce the most well-ordered materials (see Section 3.3). To test if the degree of structural ordering is also affected by reaction time, some of the syntheses were also carried out with two different reaction times, 5 and 60 minutes. A summary of the synthesis conditions is given in Table 1 (Samples 4–1 through 4–7).

The results (Table 7) show that the presence of PEHA leads to a significant increase in yield for reaction times of both 5 and 60 minutes, compared to the case where no additive is present (samples 4–4 and 4–7) as well as samples with L-arginine under equivalent conditions (samples 2–2 and 2–5, *cf.* Table 1). For both reaction times, the highest yield is achieved with PEHA at a Si : N ratio of 0.083. This suggests that PEHA addition may be an effective way to increase the yield of silica at higher ratios of Si : CTAB, where previously yields decreased but product quality improved (see Section 3.3).

Looking at the results for porosity (Table 7), the samples synthesised with PEHA generally possess somewhat lower BET surface areas and pore volumes than samples synthesised without PEHA, and this effect is enhanced at long reaction times. However, examination of the XRD data and pore size distributions (Fig. S23†) shows that, with the exception of the sample synthesised with the lowest Si : N ratio (4–3), samples synthesised with PEHA and a reaction time of 5 minutes have a markedly improved degree of order when compared with the control samples (4–4 and 4–7). Specifically, if we take porosity, yield and degree of order into consideration, a PEHA concentration of 0.083 appears to strike a good balance, yielding

materials with well-resolved reflection lines at (100), (110) and (200) that indicate hexagonally ordered mesopores with a narrow size distribution.

An increase in the reaction time had the inverse effect on samples synthesised with and without PEHA. Without any additive present, a longer reaction time seems to slightly increase the degree of order (although the difference is marginally above statistical uncertainty), in line with previous observations.[13] In contrast, the XRD patterns for samples 4–5 and 4–6, which were synthesised with PEHA present and a reaction time of 60 minutes, are significantly different from other samples. There are no discernible peaks corresponding to reflection lines at (100), (110) and (200), indicating materials with no hexagonal ordering. The shift and broadening of the peaks towards values below $2°2\theta$ suggests that these samples possess larger, amorphous pores, which is well supported by the broader pore size distributions presented in Fig. S23.† This is accompanied by a reduction in BET surface area of about 200 $m^2\ g^{-1}$. No such large mesopores are present in the corresponding sample without PEHA (4–7). This suggests that PEHA interacts with the system by a relatively slow mechanism that results in a broader pore size distribution. This may be explained by the formation of a secondary disordered porous silica phase, promoted by the presence of PEHA, which reduces the porosity of the bulk material, but occurs at a slower rate than the formation of the primary mesoporous silica phase, and therefore is not present in significant quantities at low reaction times.

Although high yields of OMS were achieved previously without the use of an additive, this necessitated the use of larger quantities of surfactant, with Si : CTAB ratios of 2 being required to achieve yields >80% when either no additive or L-arginine was used in synthesis. The use of PEHA allows for high yields to be achieved with a relatively low quantity of surfactant, *e.g.* a Si : CTAB ratio of 8. This ratio may also have benefits in terms of material structure as identified in Section 3.2. However, when reaction time is increased, there is a reduction in surface area, pore volume and degree of structural ordering. Since these phenomena happen at different time scales, it may be favorable to carry out synthesis with a low reaction time to maximize the quantity of well-ordered porous silica whilst minimizing the secondary process that reduces the degree of order in the resultant material.

This journal is © The Royal Society of Chemistry 2025

J. Mater. Chem. A, 2025, **13**, 37044–37062 | **37059**

4   Conclusions

In this work, a detailed investigation was carried out to study the effects that bio-inspired additives have on ordered mesoporous silica synthesis under mild conditions with short reaction times. Initially, a two-level four-factor design of experiments approach that utilised arginine as an additive was adopted. This identified that both pH and Si : CTAB ratio have a pronounced effect on the structural properties of the mesoporous silica obtained. A high Si : CTAB ratio appeared to be essential for well-ordered materials to be obtained, and the degree of order was significantly higher for samples synthesised at pH 7. A further investigation into the effect of component ratios identified that the most well-ordered materials were obtained with a Si : CTAB ratio of 8, while the degree of order was actually reduced as this ratio was increased to 16. Coarse-grained molecular dynamics simulations showed that the Si : CTAB ratio is critical to achieving a balance of charge at the silica/surfactant interface, which appears to be the key for achieving a well-ordered hexagonal mesophase. This structure was also shown to be significantly disrupted by changes in pH, suggesting that for well-ordered materials to be obtained as pH is lowered during synthesis, the structure formed at high pH must become "locked in" by silica condensation reactions, which proceed most rapidly at pH close to 7. While this method of "delayed neutralization" was explored by Lin et al.,[13] rapid addition of the acid appears to facilitate the formation of well-ordered materials with significantly shorter synthesis times than previously reported.

Throughout these investigations, the quantity of arginine used did not appear to have any effect on yield or material properties even when more extreme ratios of Si : N were used. In response to this, several different additives were trialled and compared to a control system in which no additive was used. Surprisingly, the control system resulted in a very well-ordered mesoporous material with a reaction time of just 5 minutes and without hydrothermal treatment. This confirmed that hydrothermal treatment is not required in order to obtain well-ordered mesoporous silica from a sodium silicate precursor, and rapid precipitation is possible simply by modifying the system pH.

The tests with alternative bio-inspired additives showed that the sample synthesised using PEHA had a higher degree of order compared with the sample synthesised with both alternative additives and no additive present. Coarse-grained molecular dynamics studies of self-assembly at high pH were carried out with both PEHA and arginine, which showed that while the self-assembly of the HLC phase is not directly affected, PEHA is readily absorbed within the silica/surfactant interface while arginine remains largely in the bulk water phase. This suggests that the role played by additives is most likely catalytic, aiding in locking in the well-ordered structure that forms during the early stages of OMS synthesis. However, to confirm this hypothesis, further experimental (e.g. measurements of reaction kinetics with and without additive) and/or computational studies (e.g. using reactive models of silica/surfactant self-assembly[60]) are necessary.

The influence of PEHA was investigated further, where it was shown that at low reaction times, the presence of smaller quantities of PEHA significantly improved both the degree of structural ordering and the synthesis yield. However, the presence of PEHA resulted in pores becoming broader and less well ordered as the reaction time or concentration of PEHA was increased. This suggests that PEHA may be used to promote the formation of well-ordered mesoporous silica particles, but reaction times must be kept low to avoid changes in the material's morphology. Due to this dual nature of the effect of PEHA on the material properties, further experimental studies, perhaps using the Design of Experiments approach we have applied with arginine, are necessary to identify the optimal conditions that lead to materials with the highest degree of order. Both high Si : N and Si : CTAB ratios are desirable from a process economics point of view, as higher ratios of silica to other components lower the quantity of reactants required, and also from a green chemistry perspective due to improved atom economy. Our work demonstrates that mesoporous silica with a high degree of order can be obtained in minutes, at room temperature, with high yield, and using small amounts of template and bio-inspired additive. This paves the way for an environmentally-friendly manufacture process of this class of materials.

Data availability

All data and codes underpinning this publication are openly available from the University of Strathclyde KnowledgeBase at **https://doi.org/10.15129/515810ae-e7e6-4d62-b688-e52b2271d31e**.

Author contributions

TS carried out synthesis and analysis of materials investigated in this work, developed computational models, conducted simulation study and drafted and edited the manuscript. CB carried out the synthesis of a preliminary sample and provided TEM imaging. SVP provided supervision of experimental work and feedback on manuscript drafts. MJ provided supervision of computational work and contributed extensive edits to manuscript.

Conflicts of interest

There are no conflicts to declare.

Acknowledgements

37060 | J. Mater. Chem. A, 2025, 13, 37044–37062

This journal is © The Royal Society of Chemistry 2025

References

1 R. Pilling and S. V. Patwardhan, Recent Advances in Enabling Green Manufacture of Functional Nanomaterials: A Case Study of Bioinspired Silica, *ACS Sustain. Chem. Eng.*, 2022, **10**, 12048–12064.

2 C. Brambila, *et al.*, A Comparison of Environmental Impact of Various Silicas Using a Green Chemistry Evaluator, *ACS Sustain. Chem. Eng.*, 2022, **10**, 5288–5298.

3 J. R. H. Manning, C. Brambila and S. V. Patwardhan, Unified mechanistic interpretation of amine—assisted silica synthesis methods to enable design of more complex materials, *Mol. Syst. Des. Eng.*, 2021, **6**, 170–196.

4 D. J. Belton, S. V. Patwardhan, V. V. Annenkov, E. N. Danilovtseva and C. C. Perry, From biosilicification to tailored materials: Optimizing hydrophobic domains and resistance to protonation of polyamines, *Proc. Natl. Acad. Sci. U. S. A.*, 2008, **105**, 5963–5968.

5 J. S. Beck, *et al.*, A new family of mesoporous molecular sieves prepared with liquid crystal templates, *J. Am. Chem. Soc.*, 1992, **114**, 10834–10843.

6 D. Zhao, Q. Huo, J. Feng, B. F. Chmelka and G. D. Stucky, Nonionic Triblock and Star Diblock Copolymer and Oligomeric Surfactant Syntheses of Highly Ordered, Hydrothermally Stable, Mesoporous Silica Structures, *J. Am. Chem. Soc.*, 1998, **120**, 6024–6036.

7 A. H. Khalbas, T. M. Albayati, N. S. Ali and I. K. Salih, Drug loading methods and kinetic release models using of mesoporous silica nanoparticles as a drug delivery system: A review, *S. Afr. J. Chem. Eng.*, 2024, **50**, 261–280.

8 R. J. Patel, *et al.*, Ordered mesoporous silica nanocarriers: An innovative paradigm and a promising therapeutic efficient carrier for delivery of drugs, *J. Drug Delivery Sci. Technol.*, 2023, **82**, 104306.

9 A. Zhu, T. Jiao, S. Ali, Y. Xu, Q. Ouyang and Q. Chen, SERS Sensors Based on Aptamer—Gated Mesoporous Silica Nanoparticles for Quantitative Detection of Staphylococcus aureus with Signal Molecular Release, *Anal. Chem.*, 2021, **93**, 9788–9796.

10 B. Sun, X. Zhen and X. Jiang, Development of mesoporous silica—based nanoprobes for optical bioimaging applications, *Biomater. Sci.*, 2021, **9**, 3603–3620.

11 A. Mohan, *et al.*, In situ thermosensitive hybrid mesoporous silica: preparation and the catalytic activities for carbonyl compound reduction, *Dalton Trans.*, 2021, **50**, 11730–11741.

12 T. Stavert, S. V. Patwardhan, R. Pilling and M. Jorge, Unlocking the holy grail of sustainable and scalable mesoporous silica using computational modelling, *RSC Sustainability*, 2023, **1**, 432–438.

13 H. P. Lin, S. Cheng and C.-Y. Mou, Synthesis of Thermally Stable MCM—41 at Ambient Temperature, *J. Chin. Chem. Soc.*, 1996, **43**, 375–378, _eprint: https://onlinelibrary.wiley.com/doi/pdf/10.1002/jccs.199600054.

14 Q. Cai, W.-Y. Lin, F.-S. Xiao, W.-Q. Pang, X.-H. Chen and B.-S. Zou, The preparation of highly ordered MCM—41 with extremely low surfactant concentration, *Microporous Mesoporous Mater.*, 1999, **32**, 1–15.

15 E. V. Vyshegorodtseva, Y. Larichev and G. V. Mamontov, The influence of CTAB/Si ratio on the textural properties of MCM—41 prepared from sodium silicate, *J. Sol-Gel Sci. Technol.*, 2019, **92**, 496–505.

16 S. V. Patwardhan and S. S. Staniland in *Green Nanomaterials, 2053-2563*, Type: Book Chapter, IOP Publishing, 2019, 9–1 to 9–25.

17 T. Yokoi, Y. Sakamoto, O. Terasaki, Y. Kubota, T. Okubo and T. Tatsumi, Periodic Arrangement of Silica Nanospheres Assisted by Amino Acids, *J. Am. Chem. Soc.*, 2006, **128**, 13664–13665.

18 M. Jorge, A. W. Milne, O. N. Sobek, A. Centi, G. Pérez-Sánchez and J. R. B. Gomes, Modelling the self—assembly of silica—based mesoporous materials, *Mol. Simul.*, 2018, **44**, 435–452.

19 G. Pérez-Sánchez, J. R. B. Gomes and M. Jorge, Modeling Self—Assembly of Silica/Surfactant Mesostructures in the Templated Synthesis of Nanoporous Solids, *Langmuir*, 2013, **29**, 2387–2396.

20 G. Pérez-Sánchez, *et al.*, Multiscale Model for the Templated Synthesis of Mesoporous Silica: The Essential Role of Silica Oligomers, *Chem. Mater.*, 2016, **28**, 2715–2727.

21 S.-C. Chien, *et al.*, Molecular Simulations of the Synthesis of Periodic Mesoporous Silica Phases at High Surfactant Concentrations, *J. Phys. Chem. C*, 2017, **121**, 4564–4575.

22 A. Centi and M. Jorge, Molecular Simulation Study of the Early Stages of Formation of Bioinspired Mesoporous Silica Materials, *Langmuir*, 2016, **32**, 7228–7240.

23 A. Centi, J. R. H. Manning, V. Srivastava, S. van Meurs, S. V. Patwardhan and M. Jorge, The role of charge—matching in nanoporous materials formation, *Mater. Horiz.*, 2019, **6**, 1027–1033.

24 R. Mee, *A Comprehensive Guide to Factorial Two—Level Experimentation*, Springer, New York, NY, 2009.

25 Y. Wan and D. Zhao, On the Controllable Soft—Templating Approach to Mesoporous Silicates, *Chem. Rev.*, 2007, **107**, 2821–2860.

26 S. Brunauer, P. H. Emmett and E. Teller, Adsorption of Gases in Multimolecular Layers, *J. Am. Chem. Soc.*, 1938, **60**, 309–319.

27 J. Rouquerol, P. Llewellyn and F. Rouquerol in *Studies in Surface Science and Catalysis*, ed. P. L. Llewellyn, F. Rodriquez-Reinoso, J. Rouqerol and N. Seaton, Characterization of Porous Solids VII, Elsevier, 2007, pp. 49–56.

28 E. P. Barrett, L. G. Joyner and P. P. Halenda, The Determination of Pore Volume and Area Distributions in Porous Substances. I. Computations from Nitrogen Isotherms, *J. Am. Chem. Soc.*, 1951, **73**, 373–380.

29 H. J. C. Berendsen, D. van der Spoel and R. van Drunen, GROMACS: A message—passing parallel molecular dynamics implementation, *Comput. Phys. Commun.*, 1995, **91**, 43–56.

This journal is © The Royal Society of Chemistry 2025

J. Mater. Chem. A, 2025, **13**, 37044–37062 | **37061**

30 A. Lindahl and v. d. S. Hess, *GROMACS 2021.5 Source Code*, 2022.

31 N. Michaud-Agrawal, E. J. Denning, T. B. Woolf and O. Beckstein, MDAnalysis: A toolkit for the analysis of molecular dynamics simulations, *J. Comput. Chem.*, 2011, **32**, 2319–2327.

32 R. J. Gowers *et al.*, MDAnalysis: A Python Package for the Rapid Analysis of Molecular Dynamics Simulations, *Proceedings of the 15th Python in Science Conference*, 2016, Conference Name: Proceedings of the 15th Python in Science Conference, pp. 98–105.

33 J. D. Hunter, Matplotlib: A 2D graphics environment, *Computing in Science & Engineering*, IEEE COMPUTER SOC, 2007, vol. 9, pp. 90–95.

34 W. L. Jorgensen, D. S. Maxwell and J. Tirado-Rives, Development and Testing of the OPLS All—Atom Force Field on Conformational Energetics and Properties of Organic Liquids, *J. Am. Chem. Soc.*, 1996, **118**, 11225–11236.

35 L. S. Dodda, I. Cabeza de Vaca, J. Tirado-Rives and W. L. Jorgensen, LigParGen web server: an automatic OPLS—AA parameter generator for organic ligands, *Nucleic Acids Res.*, 2017, **45**, W331–W336.

36 L. S. Dodda, J. Z. Vilseck, J. Tirado-Rives and W. L. Jorgensen, 1.14*CM1A—LBCC: Localized Bond—Charge Corrected CM1A Charges for Condensed—Phase Simulations, *J. Phys. Chem. B*, 2017, **121**, 3864–3870.

37 W. L. Jorgensen and J. Tirado-Rives, Potential energy functions for atomic—level simulations of water and organic and biomolecular systems, *Proc. Natl. Acad. Sci. U. S. A.*, 2005, **102**, 6665–6670.

38 H. J. C. Berendsen, J. R. Grigera and T. P. Straatsma, The missing term in effective pair potentials, *J. Phys. Chem.*, 1987, **91**, 6269–6271.

39 M. Jorge, Molecular Dynamics Simulation of Self—Assembly of n—Decyltrimethylammonium Bromide Micelles, *Langmuir*, 2008, **24**, 5714–5725.

40 M. Jorge, J. R. B. Gomes, M. N. D. S. Cordeiro and N. A. Seaton, Molecular Simulation of Silica/Surfactant Self—Assembly in the Synthesis of Periodic Mesoporous Silicas, *J. Am. Chem. Soc.*, 2007, **129**, 15414–15415.

41 M. Jorge, J. R. B. Gomes, M. N. D. S. Cordeiro and N. A. Seaton, Molecular Dynamics Simulation of the Early Stages of the Synthesis of Periodic Mesoporous Silica, *J. Phys. Chem. B*, 2009, **113**, 708–718.

42 R. W. Hockney, S. P. Goel and J. W. Eastwood, Quiet high—resolution computer models of a plasma, *J. Comput. Phys.*, 1974, **14**, 148–158.

43 G. Bussi, D. Donadio and M. Parrinello, Canonical sampling through velocity rescaling, *J. Chem. Phys.*, 2007, **126**, 014101.

44 M. Parrinello and A. Rahman, Polymorphic transitions in single crystals: A new molecular dynamics method, *J. Appl. Phys.*, 1981, **52**, 7182–7190.

45 S. Nosé and M. L. Klein, Constant pressure molecular dynamics for molecular systems, *Molecular Physics*, Taylor & Francis Group, 2006.

46 T. Darden, D. York and L. Pedersen, Particle mesh Ewald: An N·log(N) method for Ewald sums in large systems, *J. Chem. Phys.*, 1993, **98**, 10089–10092.

47 U. Essmann, L. Perera, M. Berkowitz, T. Darden, H. Lee and L. Pedersen, A Smooth Particle Mesh Ewald Method, *J. Chem. Phys.*, 1995, **103**, 8577.

48 J. A. Graham, J. W. Essex and S. Khalid, PyCGTOOL: Automated Generation of Coarse—Grained Molecular Dynamics Models from Atomistic Trajectories, *J. Chem. Inf. Model.*, 2017, **57**, 650–656.

49 P. C. T. Souza, *et al.*, Martini 3: a general purpose force field for coarse—grained molecular dynamics, *Nat. Methods*, 2021, **18**, 382–388.

50 T. Stavert, S. V. Patwardhan and M. Jorge, Development of a coarse—grained model for the early stages of ordered mesoporous silica formation, *Mol. Simul.*, 2025, **51**, 188–205.

51 L. Verlet, "Computer "Experiments" on Classical Fluids. I. Thermodynamical Properties of Lennard—Jones Molecules, *Phys. Rev.*, 1967, **159**, 98–103.

52 A. Firouzi, F. Atef, A. G. Oertli, G. D. Stucky and B. F. Chmelka, Alkaline Lyotropic Silicate–Surfactant Liquid Crystals, *J. Am. Chem. Soc.*, 1997, **119**, 3596–3610.

53 J. Šefčík and A. V. McCormick, Thermochemistry of aqueous silicate solution precursors to ceramics, *AIChE J.*, 1997, **43**, 2773–2784.

54 R. K. Iler, *The Chemistry of Silica: Solubility, Polymerization, Colloid and Surface Properties and Biochemistry of Silica*, Google-Books-ID: Dc0RAQAAIAAJ, Wiley, 1979, p. 904.

55 C. T. Kresge, M. E. Leonowicz, W. J. Roth, J. C. Vartuli and J. S. Beck, Ordered mesoporous molecular sieves synthesized by a liquid—crystal template mechanism, *Nature*, 1992, **359**, 710–712.

56 M. Thommes, *et al.*, Physisorption of gases, with special reference to the evaluation of surface area and pore size distribution (IUPAC Technical Report), *Pure Appl. Chem.*, 2015, **87**, 1051–1069.

57 J. C. Eriksson, Thermodynamics of surface phase systems: V. Contribution to the thermodynamics of the solid—gas interface, *Surf. Sci.*, 1969, **14**, 221–246.

58 P. Schneider, Adsorption isotherms of microporous—mesoporous solids revisited, *Appl. Catal., A*, 1995, **129**, 157–165.

59 N. La-Salvia, J. J. Lovón-Quintana, A. S. P. Lovón and G. P. Valença, Influence of Aluminum Addition in the Framework of MCM—41 Mesoporous Molecular Sieve Synthesized by Non—Hydrothermal Method in an Alkali—Free System, *Mater. Res.*, 2017, **20**, 1461–1469.

60 A. P. Carvalho, S. M. Santos, G. Pérez-Sánchez, J. D. Gouveia, J. R. B. Gomes and M. Jorge, Sticky—MARTINI as a reactive coarse—grained model for molecular dynamics simulations of silica polymerization, *npj Comput. Mater.*, 2022, **8**, 1–13.

37062 | *J. Mater. Chem. A*, 2025, **13**, 37044–37062

This journal is © The Royal Society of Chemistry 2025